Three dimensional flow structures in a moving droplet on substrate: A dissipative particle dynamics study

Zhen Li,[1] Guo-Hui Hu,[1,2,3] Zhi-Liang Wang,[1,2,3] Yan-Bao Ma,[4] and Zhe-Wei Zhou[1,2,3,a)]

[1]*Shanghai Institute of Applied Mathematics and Mechanics, Shanghai University, Shanghai 200072, China*
[2]*Modern Mechanics Division, E-Institutes of Shanghai Universities, Shanghai 200072, China*
[3]*Shanghai Key Laboratory of Mechanics in Energy and Environmental Engineering, Shanghai 200072, China*
[4]*School of Engineering, University of California, Merced, Merced, California 95343, USA*

(Received 2 September 2012; accepted 12 June 2013; published online 8 July 2013)

It is of both fundamental and practical interest to study the flow physics in the manipulation of droplets. In this paper, we investigate complex flow in liquid droplets actuated by a linear gradient of wettability using dissipative particle dynamics simulation. The wetting property of the substrate ranging from hydrophilic to hydrophobic is achieved by adjusting the conservative solid-liquid interactions which results in a variation of solid-liquid surface tension. The internal three-dimensional velocity field with transverse flow in droplet is revealed and analyzed in detail. When the substrate is hydrophobic, it is found that there is slight deformation but strong flow circulation inside the droplet, and the droplet rolling is the dominant mechanism for the movement. However, large deformation of the droplet is generated after the droplet reaches the hydrophilic surface, and a mechanism combining rolling and sliding dominates the transportation of the droplet. Another interesting finding is that the thermal fluctuation can accelerate the spontaneous motion of a liquid droplet under a wetting gradient. The effects of the steepness of wetting gradient and the size of droplet on the translation speed are studied as well. [http://dx.doi.org/10.1063/1.4812366]

I. INTRODUCTION

The last decade has witnessed the explosive development of microfluidic systems. Microfluidic systems allow the integration of various steps of chemical or biological analyses on a single chip, which significantly minimize reagent volume and material costs, hence attracting increasing attention since the middle of 1990s.[1] Especially, digital microfluidics has emerged as a versatile tool for applications in chemistry, biology, and medicine.[2] The manipulation of liquid droplets is one of the crucial technologies in the design and optimization of droplet-based digital microfluidics.[3,4] Therefore, it is of both fundamental and practical interest to investigate the flow physics in the manipulation of droplets.

The flows in microfluidic devices are distinguished by large surface to volume ratio and small Reynolds number, thus they are strongly influenced by surface effects and amenable to being controlled by a variety of surface effects rather than inertia or body forces.[1,5] A wetting gradient along the solid surface can create non-uniform surface tension on the circumference of a droplet base, which can be utilized to drive a droplet on a substrate.[6–9] Several different technologies have been developed for adjusting wetting properties with the purpose of manipulating droplets, including

a)Author to whom correspondence should be addressed. Electronic mail: zhwzhou@shu.edu.cn.

electrowetting on dielectric (EWOD),[10,11] light irradiation,[12,13] thermal gradient,[6,14] microstructure geometry,[15,16] and chemical outmost layer.[9,17]

The motion of a droplet actuated by the gradient of wettability has been investigated in experiments.[13,16,18] Moumen *et al.*[18] measured the velocity of a droplet along a gradient surface. It was found that the velocity rises to a peak in the first few millimeters and decays by an order of magnitude as it moves into the more hydrophilic region. Lai *et al.*[16] proposed an approach to fabricate a solid surface to generate a gradient from superhydrophobic to hydrophilic and studied the transportation of a droplet. Gao and McCarthy[19] pointed out that droplets may move by sliding, rolling, or some combination of these two extremes, but this supposition has not been explicitly demonstrated. To explore the flow physics inside a moving droplet, Kinoshita *et al.*[20] used the confocal micro particle image velocimetry (μ-PIV) system to study the internal flow of a droplet in a microchannel. Lu *et al.*[21] reported the internal flow of a thick droplet actuated by EWOD. They reconstructed the three-dimensional (3D) velocity field from the two-dimensional (2D) μ-PIV experimental data by solving the continuity equation. Nevertheless, it is still challenging to design experiments to visualize the flow fields inside a moving droplet.

With the development of numerical techniques and advanced computers, numerical simulations have become an indispensable tool for the study of complex fluid phenomena. Shi *et al.*[22] and Das *et al.*[23,24] studied the 2D internal flow structure of a liquid drop over a solid surface and found a strong circulation inside the moving droplet. So far, there are relatively fewer investigations on 3D flow structures in a moving droplet.

The 3D simulation of a liquid droplet moving on a solid surface constitutes a considerable level of complexity. Apart from the three dimensionality of the problem, a common difficulty experienced by analytical models and numerical schemes is the stress singularity at the triple contact line.[23] For modeling a liquid droplet on a solid surface, it is difficult for grid-based Navier-Stokes simulators to directly use interface tracking algorithms such as the front tracking method, the volume of fluid method, and the level set method near the triple line.[25] A number of remedies, such as incorporation of precursor film,[26] surface tension relaxation,[27] and slip length based approach,[28] have been utilized to consider the singularity associated with the triple contact line. Alternatively, dissipative particle dynamics (DPD), a grid-free particle-based simulation method, has been successfully used in modeling capillary wetting[29,30] and multiphase flows.[25,31] Cupelli *et al.*[30] reported that this particle-based method provides a natural way of avoiding the stress singularity at the triple line. In the present work, the DPD is employed to simulate the movement of a liquid droplet on a flat solid surface.

For fluids in sub-micrometer/nano scale, thermal fluctuations become significant and could affect the dynamical behaviors, such as breakup of nanojets, wetting and spreading processes of droplets.[32–35] To consider thermal fluctuation, Davidovitch *et al.*[32] investigated the spreading of a droplet on a substrate by utilizing stochastic lubrication equation. They found that the presence of thermal fluctuation will enhance the droplet spreading, which was also confirmed by atomistic simulation.[31] However, to the best of our knowledge, the influence of thermal fluctuation on the movement of a droplet on a wetting gradient has not been addressed before. DPD is a proper technique to explore this problem since thermal fluctuation is intrinsically considered in the algorithm.

The main objective of this paper is to reveal the 3D internal flow field of a moving droplet on a wetting gradient, as well as to investigate the influence of thermal fluctuation on the movement of the droplet. The algorithm of DPD is introduced in Sec. II. The results of the numerical simulations are discussed in Sec. III. Finally, some concluding remarks are made in Sec. IV.

II. DISSIPATIVE PARTICLE DYNAMICS SIMULATION

DPD was proposed by Hoogerbrugge and Koelman[36] to take the advantages of large timescale in lattice-gas automata (LGA) and mesh-free algorithm in molecular dynamics (MD). The basic component of DPD is coarse-grained particle which represents cluster of molecules instead of atoms/molecules themselves.

The time evolution of a DPD particle i with unit mass follows the Newton's laws of motion given by

$$\begin{aligned} \frac{d\mathbf{r}_i}{dt} &= \mathbf{v}_i, \\ \frac{d\mathbf{v}_i}{dt} &= \mathbf{F}_i = \sum_{i \neq j} \left(\mathbf{F}_{ij}^C + \mathbf{F}_{ij}^D + \mathbf{F}_{ij}^R\right), \end{aligned} \tag{1}$$

where t, $\mathbf{r}_i$, $\mathbf{v}_i$, and $\mathbf{F}_i$ denote time, position, velocity, and force vectors, and $\mathbf{F}_{ij}^C$, $\mathbf{F}_{ij}^D$, and $\mathbf{F}_{ij}^R$ represent the conservative, dissipative, and random forces, respectively. The summation is carried out over all other particles within a cutoff radius r_c.

The dissipative or the drag force $\mathbf{F}_{ij}^D$ is given by $\mathbf{F}_{ij}^D = -\gamma\omega_D(r_{ij})(\mathbf{e}_{ij} \cdot \mathbf{v}_{ij})\mathbf{e}_{ij}$, where γ is dissipative parameter, ω_D is a weight function, r_{ij} is distance between particles i and j, $\mathbf{e}_{ij}$ is the unit vector from particle j to i, and $\mathbf{v}_{ij} = \mathbf{v}_i - \mathbf{v}_j$ is the velocity difference. The random force is written as $\mathbf{F}_{ij}^R = \delta\omega_R(r_{ij})\xi_{ij}\Delta t^{-1/2}\mathbf{e}_{ij}$, where ξ_{ij} is the Gaussian white noise with zero mean and unit variance. It describes the degrees of freedom that have been eliminated from the coarse-graining process. The dissipative force and random force act as a thermostat if the dissipation parameter γ and the amplitudes of white noise δ satisfy the fluctuation-dissipation theorem[37] requiring $\delta^2 = 2\gamma k_B T$ and $\omega_D(r) = [\omega_R(r)]^2$, in which k_B is the Boltzmann constant and T is the temperature determined by the DPD thermostat.

The conservative force $\mathbf{F}_{ij}^C$ between particle i and particle j is responsible for the thermodynamic behavior of the system. It usually reads $\mathbf{F}_{ij}^C = \alpha_{ij}\omega_C(r_{ij})\mathbf{e}_{ij}$ in standard DPD, where α_{ij} is a repulsive force parameter, ω_C is a soft and unspecific weight function. A common choice of the weight function is $\omega_C = 1 - r_{ij}/r_c$ for $r_{ij} \leq r_c$ and $\omega_C = 0$ for $r_{ij} > r_c$. It is worth noting that this conservative force contains only the repulsive force. As a result, the Equation of State (EOS) of the system becomes a quadratic function of the particle densityρ,[38] which excludes the possibility of simulating phenomena with liquid-vapor interfaces.

To simulate the interfacial phenomena, many-body DPD (MDPD) was developed by modifying the expression of the conservative force.[29–31,39,40] In the approach developed by Warren,[40] the density-dependent conservative force is introduced empirically with a different cut-off radius r_d, and can be written as

$$\mathbf{F}_{ij}^C = A_{ij}\omega_C(r_{ij})\mathbf{e}_{ij} + B(\bar{\rho}_i + \bar{\rho}_j)\omega_d(r_{ij})\mathbf{e}_{ij}, \tag{2}$$

where the first term with the species-dependent constant $A_{ij} < 0$ stands for an attractive force within an interaction range r_c. A_{ll} describes the interaction between liquid (l) and liquid (l) particles, while A_{sl} stands for the interaction between solid (s) particles and liquid (l) particles. The second term with $B > 0$ is the density-dependent repulsive force within an interaction range r_d. The local density ρ_i at the location of particle i can be recovered by the instantaneously weighted average[40] $\rho_i = \sum_{i \neq j} \omega_\rho(r_{ij})$ with $\omega_\rho = 15/(2\pi r_d^3)(1 - r_{ij}/r_d)^2$.

We use reduced units that are quite standard for DPD, i.e., length in r_c, energy in $k_B T$, and mass in m. All quantities are defined following the choice of Refs. 29, 30, and 40, as listed in Table I.

TABLE I. The computational parameters used in the present simulations. All quantities are given in DPD units.

Parameters	Symbol	Value
Particle density	ρ	6.00
Cut-off radius of attractive force	r_c	1.00
Cut-off radius of repulsive force	r_d	0.75
Time step	Δt	0.01
System temperature	$k_B T$	1.00
Amplitude of white noise	δ	6.00
Attraction parameter	A_{ll}	− 40.00
Repulsion parameter	$B_{ll} = B_{sl}$	25.00

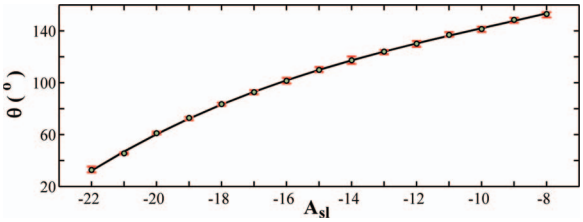

FIG. 1. Static contact angle θ is adjusted from hydrophilic to hydrophobic with the variation of A_{sl}. Other parameters of the DPD fluid are given in Table I.

Since the droplet simulated with a radius less than capillary length, which is usually few millimeters, the gravity is not considered in the present study. Simulations are performed in a three-dimensional computational region of size $160 \times 60 \times 60$. A liquid drop of radius $R = 10$ containing 25 396 fluid particles is placed on a flat solid wall, which is constructed by three frozen layers with 75 762 wall particles. To satisfy the no-slip boundary condition, bounce-back reflection is used when the fluid particles penetrate the wall.[41] As addressed by Cupelli *et al.*,[30] no contact line model is used in the algorithm. The periodic boundary conditions are applied in both x and y directions. A modified velocity-Verlet algorithm[38] is utilized for the numerical integration of the many-body DPD equations with time step $\Delta t = 0.01$ and the variable factor $\lambda = 0.65$. The solid-vapor (sv), solid-liquid (sl), and liquid-vapor interfacial tensions are output properties and can be measured independently.[30]

The wetting behavior is allowed to adjust from hydrophilic to hydrophobic by changing the mutual attraction between the solid and liquid particles, which results in variation of the solid-liquid interfacial tension. As displayed in Fig. 1, the static contact angle θ is a monotonous function of A_{sl}. Giving a location-dependent A_{sl} in the form of

$$\mathrm{A}_{sl} = \begin{cases} -8.662 & x < -40 \\ 1.03 \times 10^{-3}x^2 - 0.16x - 16.71 & -40 \le x \le 40 \\ -21.462 & x > 40 \end{cases}, \tag{3}$$

which results in the static contact angle $\theta_L = 150^\circ$ for $x < -40$ and $\theta_R = 40^\circ$ for $x > 40$, and a linear gradient of contact angle varying from θ_L to θ_R between -40 and 40 in x direction, as shown in Fig. 2.

To validate the DPD model of a droplet on a wetting gradient, a droplet driven by wetting gradient in two-dimension, as shown in Fig. 3, is studied. If the inertial effects and contact angle hysteresis are ignored, the quasisteady velocity of the nondeformable droplet can be theoretically given by[6]

$$V = \frac{\sigma_{lv}\theta_D}{6\mu l}(\cos\theta_a - \cos\theta_b), \tag{4}$$

where μ is the fluid viscosity, σ_{lv} is the liquid-vapor interfacial tension, θ_a and θ_b are the equilibrium contact angles at the advancing and receding edges, respectively. θ_D is the average dynamic contact angle given by $2\cos(\theta_D) = \cos(\theta_a) + \cos(\theta_b)$. l is a parameter defined by $l = \ln(x_{\max}/x_{\min})$ in

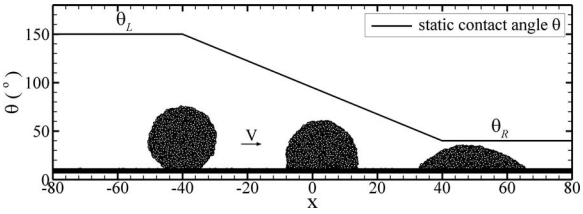

FIG. 2. The computational model.

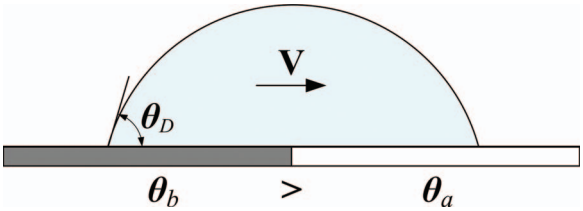

FIG. 3. A liquid droplet on a wetting gradient with $\theta_b > \theta_a$ in two dimension.

which x_{max} is half the base length of the droplet and x_{min} is a molecular size which enters as the cutoff length in the calculation.[42]

To validate the present algorithm, the comparison between the DPD simulations and theoretical predictions by (4) is shown in Fig. 4. Obviously the translation speed obtained by the DPD model is well consistent with the theoretical results.

III. RESULTS AND DISCUSSION

When a spherical droplet is released on a heterogeneous substrate, the wetting gradient across the droplet induces a resultant force on the droplet hence actuates it towards the hydrophilic end, as shown in Fig. 2. The center-of-mass position X_{CM} and its velocity of the droplet V varying with time are plotted in Fig. 5. The variation of V with time is qualitatively consistent with the experiment by Moumen *et al.*[18]

A dimensionless parameter, aspect ratio $\alpha = H/L$, which is defined as the maximal vertical height over maximal horizontal length of the liquid droplet, is used to describe the deformation of the droplet during the movement. $\alpha = 1.0$ represents a sphere while small α means spherical cap. As shown in Fig. 5(b), the movement of the droplet can be roughly divided into three stages by analyzing the variation of α. In the beginning stage (stage 1), the speed of droplet increases rapidly when the factor α changes slightly, which indicates that the droplet has little deformation in this stage. After the speed of droplet V reaches its maximum, it begins to decelerate and the aspect ratio α declines rapidly (stage 2). Obviously, as the droplet moves on the wetting gradient, the solid-liquid surface tension increases while the contact angles decrease, the droplet becomes a spherical cap in the end of the stage. The dissipated energy will exceed the loss of the surface energy and this results in the reduction of V. In the final stage (stage 3), the area of liquid-solid interface raises dramatically due to the deformation of droplet. This consequently leads to the increasing of viscous drag and slow down the movement of droplet.

After the droplet is released, the droplet-substrate system tends to minimize its surface energy, which results in the movement of the droplet. Some of the energy is consumed by the viscous dissipation while some convert into the kinetic energy of the droplet. Figure 6 describes the time history of the surface energy, as well as the translation part of the kinetic energy of the moving

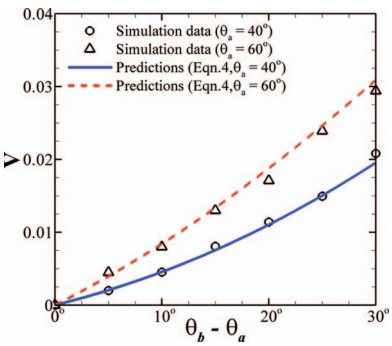

FIG. 4. Comparison between DPD simulations and theoretical predictions.

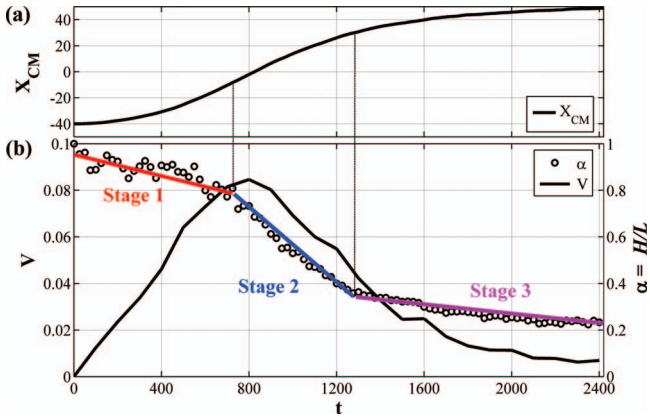

FIG. 5. The variation of (a) the center-of-mass position X_{CM} and (b) the velocity of the droplet V and the aspect ratio α with time. The droplet-substrate system is given as Fig. 2 with $\theta_L = 150^\circ$ and $\theta_R = 40^\circ$.

droplet. E_K is the translational kinetic energy of the moving droplet given by $E_K = \sum m_i \cdot V^2/2$ in which V is the velocity of the droplet. E_S is the surface energy of the droplet. Both E_K and E_S have been scaled by the initial surface energy of the droplet E_{S0}. The variation of surface energy E_S is given by $dE_s = \sigma_{lv} dS_{lv} + \sigma_{sv} dS_{sv} + \sigma_{ls} dS_{sl}$, in which l, v, and s stands for liquid, vapor, and solid, respectively, σ_{ij} is surface tension and S_{ij} is contact area. Since $dS_{sv} = -dS_{sl}$, using Young equation, for a local equilibrium contact angle θ, it yields $dE_s = \sigma_{lv}(dS_{lv} - \cos\theta_C dS_{sl})$. $\sigma_{lv} = 7.53$ is obtained following Ref. 30. For simplification, θ_C is assumed to be the equilibrium contact angle at the x- position of center-of-mass. To estimate the value of S_{lv} and S_{sl} the droplet is supposed to be a spherical cap with fixed volume.

As the droplet moves on the surface, the unbalance Young force results in the variation of its surface energy. At the beginning of the movement, the loss rate of the surface energy is small but still enough to initiate the movement of the droplet. The increase of E_K means the acceleration of the droplet while the decrease of E_K indicates the deceleration of the droplet. During the movement of the droplet the change of surface energy is $0.64E_{S0}$, while the maximum E_K is only 0.9% of E_{S0}, which implies that most of surface energy is consumed by dissipation and reveals that the surface effects are much more important than the inertial effect in the present simulations. Corresponding to Fig. 5, the reduction of surface energy accelerates the droplet in the first stage until the velocity of the droplet reaches its maximum. Then the movement of droplet leads to the increase of dissipative energy, thus the droplet slows down in the second stage. In the third stage, the surface energy nearly does not change anymore and viscous resistance finally stops the translation of the droplet.

The rate of change of the dissipative energy E_D can be calculated using the formula in Ref. 43. The time evolution of E_D is obtained by integrating its rate of change over time, as shown in the dashed-dotted line of Fig. 6. It reveals that the dissipation becomes significant only in

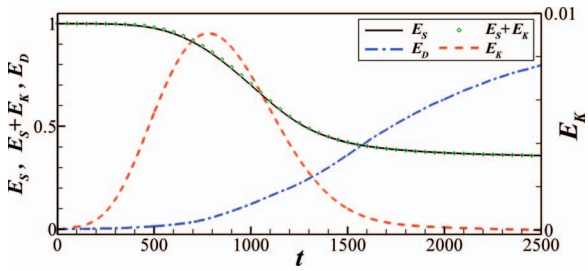

FIG. 6. The time history of the surface energy (solid line), the translation part of the kinetic energy (dashed line – red) and their sum (circles – green), as well as the dissipative energy (dashed-dotted line – blue) of the moving droplet. E_S, E_K, and E_D are scaled by the initial surface energy E_{S0}.

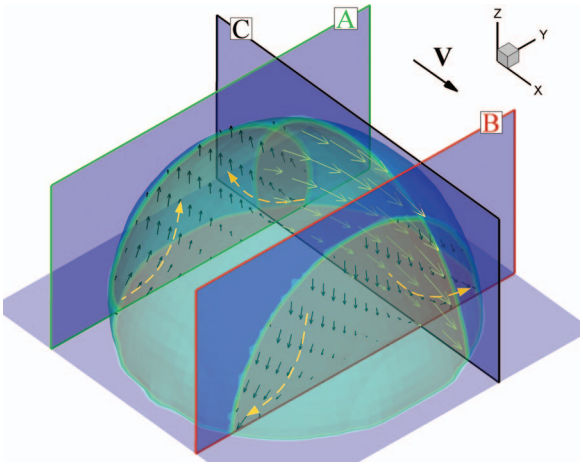

FIG. 7. The three-dimensional velocity field of the moving droplet. The dashed arrows on sections A and B sketch the flow direction on each section. Vector V denotes the droplet moving direction.

stages 2 and 3. However, the total dissipative energy of $0.8E_{S0}$ is larger than the change of surface energy of $0.64E_{S0}$ which is responsible for the movement of droplet. The reason is that, in the present version of the DPD algorithm, the dissipative force reduces the velocity difference between particles hence dissipates the thermal kinetic energy of the system, while the random force generates stochastic force on particles and provides energy. They satisfy the fluctuation-dissipation theorem and act as a thermostat to maintain the system at a constant temperature. In other words, the DPD system is an isothermal system and does not conserve energy.[43] Thus the obtained dissipative energy is overestimated. To accurately analyze the energy consumption in a moving droplet a version of energy conservative DPD might be a better choice.

The internal flow field of the moving droplet has to be examined to understand the process of the drop movement. To obtain the statistically steady velocity field in the droplet, the fluctuation in velocity should be removed from the transient numerical results of DPD. A quasi-stationary state, in which the droplet is forced to move with a constant speed without shape changing, is generated, aiming at obtaining the flow field by time averaging. In the simulations, this is fulfilled by applying and keeping a fixed wettability gradient on the droplet as the droplet moves. It is found that the shape and the speed of the droplet keep constant after some relaxation time steps during the simulation.

To obtain the local velocity vectors from the numerical results, the computational domain is divided into cubical cells. The local velocities are obtained by averaging the sampled data over sufficient time steps at each cubic cell. When the droplet moves to the location of $X_{CM} = -5.8$, the transition from stage 1 to stage 2 is exhibited. The static contact angle across the droplet varies from hydrophobic (118° at the posterior end) to hydrophilic (85° at the anterior end) in x direction. Figure 7 depicts the three-dimensional velocity field in the moving droplet, in which the velocity vectors are projected in cross sections A, B, and C. It can be found that the contact angle is a sharp angle at anterior section B, whereas it is an obtuse angle at posterior section A. The velocity vectors indicate that the fluid particles at Section B tend to spread on the hydrophilic wall, while the particles at section A are inclined to leave the solid wall. Consequently, the liquid droplet moves towards the hydrophilic region. It is worth mentioning that as a coarse graining method DPD does not have enough resolution near contact line in dynamical processes, though Cupelli *et al.*[30] generated a stationary situation and successfully extracted the flow field near contact line from DPD simulation.

Shi *et al.*[22] and Das *et al.*[24] simulated the fluid motion inside a drop over a substrate and found strong circulation in the two-dimensional velocity field of the drop. In the present study, the vortical structure of internal flow is presented after subtracting the translational velocity V of droplet from the three-dimensional velocity field, as shown in Fig. 8. The droplet moves along positive axis x and the surface of half droplet is illustrated. Result obtained reveals that the droplet moves by a combination of rolling and sliding. Four trajectories of fluid particles in the internal flow are plotted,

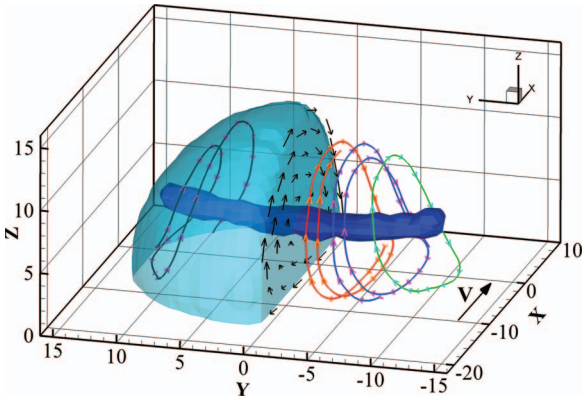

FIG. 8. The three-dimensional flow structure inside the moving droplet, in which the velocity of the droplet has been subtracted. The horizontal dark shape (blue) denotes the vortex center of each section.

and the velocity vectors on central section $Y = 0$ are presented as well. It can be seen that each trajectory has three-dimensional structures instead of staying in a plane, which reveals that there are transverse mass transportations inside the droplet. The oblique trajectories imply the existence of transverse flow in y direction, which is perpendicular to moving direction of droplet. Farther away from the central section, the transverse flow is stronger and which might be benefit for the liquid mixing inside the moving droplet. However, near the central section, the transverse velocity component is small. Thus the velocity fields of central section $Y = 0$ are utilized to describe the flow structure.

Figure 9 depicts the flow vectors of the central section $Y = 0$ when the whole droplet locates on hydrophobic surface at $X_{CM} = -27$ and between the hydrophobic and hydrophilic surfaces at $X_{CM} = -5.8$. The velocity profiles on three auxiliary lines are plotted with black color. Both results manifest a solid-core like vortex in the internal flow. However, Figure 9(a) reveals that the droplet on the hydrophobic substrate moves like a rolling sphere, with relatively smaller area of solid-liquid interface. The rolling brings about less viscous dissipation, thus results in the rising of translation velocity. In comparison, the shape of droplet on hydrophilic substrate, as shown in Fig. 9(b), is nearly a hemi-sphere. Larger shear stress and solid-liquid contacting area induce profound viscous drag, therefore slow down the movement of the droplet.

The self-transport behavior of droplet can be also influenced by gradient steepness and the droplet size. To study the effect of gradient steepness, the static contact angle at the left side of

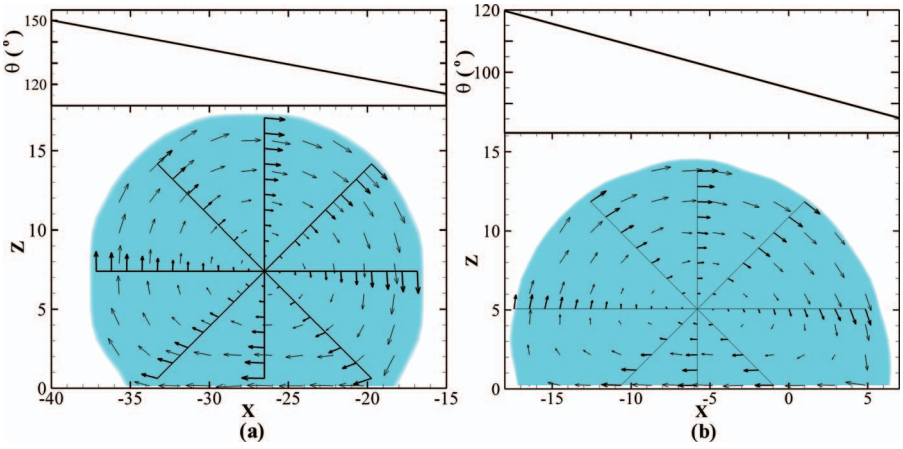

FIG. 9. The structure of velocity field of the central section $Y = 0$, (a) droplet locates on hydrophobic surface at $X_{CM} = -27$ and (b) droplet crosses hydrophobic and hydrophilic surfaces at $X_{CM} = -5.8$. The velocity of droplet has been subtracted.

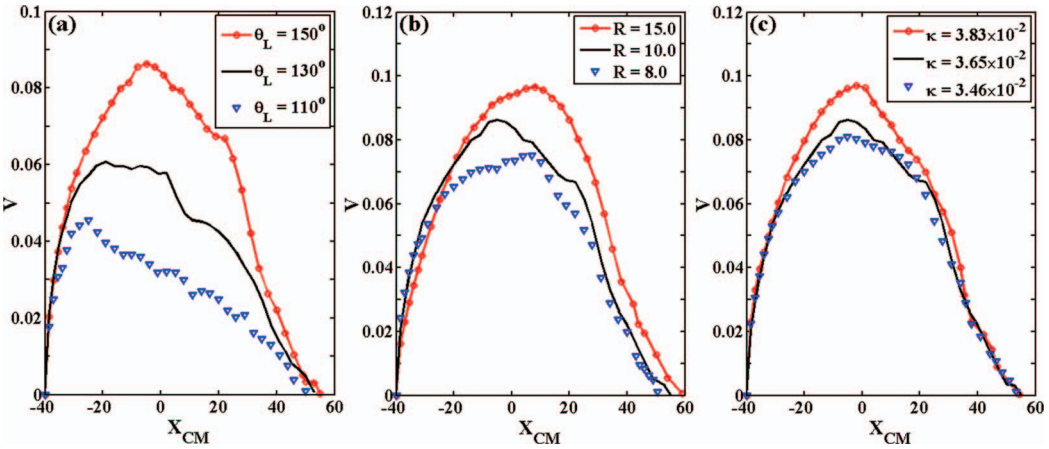

FIG. 10. Effect of (a) strength of wetting gradient, (b) droplet size, and (c) thermal fluctuation on the self-transport process actuated by linear gradient of wettability.

the substrate θ_L in Fig. 2 is allowed to vary from 150° to 130° while the static contact angle at the right side is fixed by $\theta_R = 40°$ in the present study. The droplet starts to move towards the right side after it is released at $X_{CM} = -40$ and accelerates to a maximum velocity, then slows down and comes to halt after there is no difference of wettability across the droplet. As predicted, the curves in Fig. 10(a) reveal that the translation velocity of droplet increases with larger gradient. The effect of droplet size is illustrated in Fig. 10(b) by considering three droplets with radius $R = 8.0$, 10.0, and 15.0, respectively. It is found that larger droplet can reach a higher maximum of speed than the smaller ones and finally arrive at the destination sooner, which is agreed with the experiment of Zielke and Szymczyk.[13] This might be ascribed to that the driving surface force is stronger for droplets with larger radius because the difference of wettability across the droplet is bigger due to its larger solid-liquid interface.

Thermal fluctuation could be a crucial factor to affect dynamics of fluids at small scales.[33] This have been confirmed by previous studies on breakup and formation of nanojets,[34] spreading of droplet,[32] as well as dewetting of thin films.[34] The thermal fluctuation in a DPD system is generated by the stochastic force between particles. The temperature-dependent amplitude δ is given by $\delta^2 = 2\gamma k_B T$, which is allowed to be changed to consider the effect of thermal fluctuation. The initial $k_B T$ is chose to be the energy unit for scaling the DPD system and a 10% variation of $k_B T$ is considered. A dimensionless number κ is utilized to characterize the importance of thermal fluctuations. κ is the ratio of the thermal capillary length[34] $l_T = \sqrt{k_B T / \sigma_{lv}}$, in which σ_{lv} is the liquid-vapor surface tension, to the radius of the droplet R, given by $\kappa = l_T / R$. It describes the importance of the temperature-dependent fluctuation in the movement of the droplet. Larger value of κ means higher thermal fluctuation level. Figure 10(c) shows that the influences of the thermal fluctuation on the velocity of the droplet. It indicates that the thermal fluctuation is helpful to accelerate the transportation of the droplet, especially when the velocity of the droplet reaches its maximum. A possible reason is that the thermal fluctuation increases the mobility of the DPD particles hence the droplet needs less time for spreading. However, the thermal fluctuation does not affect the location where the droplet finally stops.

IV. CONCLUSIONS

The physics of moving liquid droplets on a solid substrate driven by a linear gradient of wettability has been investigated using DPD method. When a spherical droplet was released on a wetting gradient, a driving force on the droplet was generated by the non-uniform surface tension. According to the evolution of droplet shape, the process of the movement was divided into three stages. In the first stage, the reduction of surface energy leads to the acceleration of droplet. In the meantime, the rolling dominates the movement and the droplet has little deformation. In the second

stage, viscous friction increases due to the movement of droplet, which results in the deceleration of droplet in the second stage. There is noticeable deformation on the droplet shape and an increase in liquid-solid interface area. This further raises the dissipative energy in the droplet translation. In the third stage, the surface energy does not decease anymore. A part of the droplet moves out of the region with surface wetting gradient and the driving force vanishes. Consequently, the droplet decelerates with slight deformation and comes to halt.

The 3D internal flow field of a moving droplet on a wetting gradient has been analyzed. A vortical structure was visualized after the translation velocity V was subtracted. The vortex core of the droplet on a hydrophobic surface indicates that the droplet rotates like a solid body. Velocity field shows that the fluid particles flow downwards and spread in the anterior end whereas they move upwards and leave the solid wall in the posterior end. The streamlines splay substantially, indicating the existence of transverse flow inside the moving droplet. Additionally, the transverse flow is stronger farther away from the central section.

The effects of thermal fluctuation, gradient steepness, and droplet size on the dynamics of droplet have been investigated. It was found that the increase of gradient steepness and droplet size can accelerate the droplet movement. The increase of thermal fluctuation is also capable of assisting the transportation of droplet, but it has no effect on the location where the droplet stops.

The results obtained in this study not only help us to understand the complex flow physics inside moving liquid droplets but also provide a guidance for optimal design of digital microfluidic for manipulation of droplets.

ACKNOWLEDGMENTS

This work was supported by the National Science Foundation of China (Grant Nos. 10872122 and 11272197), Doctoral Fund of Ministry of Education of China (Grant No. 20103108110004), and Shanghai Program for Innovative Research Team in Universities. We thank two referees for their valuable suggestions to improve our manuscript.

[1] A. A. Darhuber and S. M. Troian, "Principles of microfluidic actuation by modulation of surface stresses," Annu. Rev. Fluid Mech. **37**, 425 (2005).
[2] R. B. Fair, "Digital microfluidics: is a true lab-on-a-chip possible?," Microfluid. Nanofluid. **3**, 245 (2007).
[3] H.-B. Nguyen and J.-C. Chen, "A numerical study of thermocapillary migration of a small liquid droplet on a horizontal solid surface," Phys. Fluids **22**, 062102 (2010).
[4] R. Seemann, M. Brinkmann, T. Pfohl, and S. Herminghaus, "Droplet based microfluidics,"Rep. Prog. Phys. **75**, 016601 (2012).
[5] J. Atencia and D. J. Beebe, "Controlled microfluidic interfaces," Nature (London) **437**, 648 (2005).
[6] F. Brochard, "Motions of droplets on solid surfaces induced by chemical or thermal gradients," Langmuir **5**, 432 (1989).
[7] H. P. Greenspan, "On the motion of a small viscous droplet that wets a surface,"J. Fluid Mech. **84**, 125 (1978).
[8] E. Raphaël, "Spreading of droplets on a patchy surface," C. R. Acad. Sci., Ser. II: Mec., Phys., Chim., Sci. Terre Univers **306**, 751 (1988).
[9] M. K. Chaudhury and G. M. Whitesides, "How to make water run uphill," Science **256**, 1539 (1992).
[10] M. G. Pollack, R. B. Fair, and A. D. Shenderov, "Electrowetting-based actuation of liquid droplets for microfluidic applications," Appl. Phys. Lett. **77**, 1725 (2000).
[11] J. Lee and C. J. Kim, "Surface-tension-driven microactuation based on continuous electrowetting," J. Microelectromech. Syst. **9**, 171 (2000).
[12] K. Ichimura, S. K. Oh, and M. Nakagawa, "Light-driven motion of liquids on a photoresponsive surface," Science **288**, 1624 (2000).
[13] P. C. Zielke and J. A. Szymczyk, "Experimental investigation of the motion and deformation of droplets on surfaces with a linear wettability gradient," Eur. Phys. J. Spec. Top. **166**, 155 (2009).
[14] R. H. Farahi, A. Passian, T. L. Ferrell, and T. Thundat, "Microfluidic manipulation via Marangoni forces," Appl. Phys. Lett. **85**, 4237 (2004).
[15] S. Shibuichi, T. Onda, N. Satoh, and K. Tsujii, "Super water-repellent surfaces resulting from fractal structure," J. Phys. Chem. **100**, 19512 (1996).
[16] Y.-H. Lai, J.-T. Yang, and D.-B. Shieh, "A microchip fabricated with a vapor-diffusion self-assembled-monolayer method to transport droplets across superhydrophobic to hydrophilic surfaces," Lab Chip **10**, 499 (2010).
[17] T. G. Ruardy, J. M. Schakenraad, H. C. van der Mei, and H. J. Busscher, "Preparation and characterization of chemical gradient surfaces and their application for the study of cellular interaction phenomena," Surf. Sci. Rep. **29**, 3 (1997).
[18] N. Moumen, R. S. Subramanian, and J. B. McLaughlin, "Experiments on the motion of drops on a horizontal solid surface due to a wettability gradient," Langmuir **22**, 2682 (2006).
[19] L. C. Gao and T. J. McCarthy, "Contact angle hysteresis explained," Langmuir **22**, 6234 (2006).

[20] H. Kinoshita, S. Kaneda, T. Fujii, and M. Oshima, "Three-dimensional measurement and visualization of internal flow of a moving droplet using confocal micro-PIV," Lab Chip **7**, 338 (2007).
[21] H.-W. Lu, F. Bottausci, J. D. Fowler, A. L. Bertozzi, C. Meinhart, and C.-J. Kim, "A study of EWOD-driven droplets by PIV investigation," Lab Chip **8**, 456 (2008).
[22] Z.-Y. Shi, G.-H. Hu, and Z.-W. Zhou, "Lattice Boltzmann simulation of droplet motion driven by gradient of wettability," Acta Phys. Sin. **59**, 2595 (2010).
[23] A. K. Das and P. K. Das, "Simulation of drop movement over an inclined surface using smoothed particle hydrodynamics," Langmuir **25**, 11459 (2009).
[24] A. K. Das and P. K. Das, "Multimode dynamics of a liquid drop over an inclined surface with a wettability gradient," Langmuir **26**, 9547 (2010).
[25] M. Liu, P. Meakin, and H. Huang, "Dissipative particle dynamics simulation of pore-scale multiphase fluid flow," Water Resour. Res. **43**, W04411, doi:10.1029/2006WR004856 (2007).
[26] P. G. de Gennes, "Wetting: statics and dynamics," Rev. Mod. Phys. **57**, 827 (1985).
[27] Y. D. Shikhmurzaev, "Moving contact lines in liquid/liquid/solid systems," J. Fluid Mech. **334**, 211 (1997).
[28] P. D. M. Spelt, "A level-set approach for simulations of flows with multiple moving contact lines with hysteresis," J. Comput. Phys. **207**, 389 (2005).
[29] S. Merabia and I. Pagonabarraga, "A mesoscopic model for (de)wetting," Eur. Phys. J. E **20**, 209 (2006).
[30] C. Cupelli, B. Henrich, T. Glatzel, R. Zengerle, M. Moseler, and M. Santer, "Dynamic capillary wetting studied with dissipative particle dynamics," New J. Phys. **10**, 043009 (2008).
[31] A. Tiwari and J. Abraham, "Dissipative-particle-dynamics model for two-phase flows," Phys. Rev. E **74**, 056701 (2006).
[32] B. Davidovitch, E. Moro, and H. A. Stone, "Spreading of viscous fluid drops on a solid substrate assisted by thermal fluctuations," Phys. Rev. Lett. **95**, 244505 (2005).
[33] M. Rauscher and S. Dietrich, "Wetting phenomena in nanofluidics," Annu. Rev. Mater. Res. **38**, 143 (2008).
[34] M. Moseler and U. Landman, "Formation, stability, and breakup of nanojets," Science **289**, 1165 (2000).
[35] K. Mecke and M. Rauscher, "On thermal fluctuations in thin film flow," J. Phys.: Condens. Matter **17**, S3515 (2005).
[36] P. J. Hoogerbrugge and J. M. V. A. Koelman, "Simulating microscopic hydrodynamic phenomena with dissipative particle dynamics," Europhys. Lett. **19**, 155 (1992).
[37] P. Español and P. Warren, "Statistical mechanics of dissipative particle dynamics," Europhys. Lett. **30**, 191 (1995).
[38] R. D. Groot and P. B. Warren, "Dissipative particle dynamics: Bridging the gap between atomistic and mesoscopic simulation," J. Chem. Phys. **107**, 4423 (1997).
[39] I. Pagonabarraga and D. Frenkel, "Dissipative particle dynamics for interacting systems," J. Chem. Phys. **115**, 5015 (2001).
[40] P. B. Warren, "Vapor-liquid coexistence in many-body dissipative particle dynamics," Phys. Rev. E **68**, 066702 (2003).
[41] M. Revenga, I. Zuniga, and P. Espanol, "Boundary model in DPD," Int. J. Mod. Phys. C **09**, 1319 (1998).
[42] J. D. Halverson, C. Maldarelli, A. Couzis, and J. Koplik, "A molecular dynamics study of the motion of a nanodroplet of pure liquid on a wetting gradient," J. Chem. Phys. **129**, 164708 (2008).
[43] P. Español, "Dissipative particle dynamics with energy conservation," Europhys. Lett. **40**, 631 (1997).